RESEARCH ARTICLE

Thermal, Spectroscopic, and *Ab Initio* Structural Characterization of Carprofen Polymorphs

GIOVANNA BRUNI,[1] FABIA GOZZO,[2] DORETTA CAPSONI,[1] MARCELLA BINI,[1] PIERO MACCHI,[3] PETRA SIMONCIC,[2,3] VITTORIO BERBENNI,[1] CHIARA MILANESE,[1] ALESSANDRO GIRELLA,[1] STEFANIA FERRARI,[1] AMEDEO MARINI[1]

[1]C.S.G.I. Department of Physical Chemistry "M. Rolla", Pavia 27100, Italy

[2]Paul Scherrer Institut, Swiss Light Source, Villigen PSI 5232, Switzerland

[3]Department of Chemistry and Biochemistry, University of Bern, Bern CH3012, Switzerland *For thermal and spectroscopic investigations correspondence* to: Giovanna Bruni (Telephone: +39-0382-987667; Fax: +39-0382-987670; E-mail: giovanna.bruni@unipv.it)

Received 10 June 2010; revised 28 October 2010; accepted 7 December 2010

Published online in Wiley Online Library (wileyonlinelibrary.com). DOI 10.1002/jps.22470

ABSTRACT: Commercial and recrystallized polycrystalline samples of carprofen, a nonsteroidal anti-inflammatory drug, were studied by thermal, spectroscopic, and structural techniques. Our investigations demonstrated that recrystallized sample, stable at room temperature (RT), is a single polymorphic form of carprofen (polymorph I) that undergoes an isostructural polymorphic transformation by heating (polymorph II). Polymorph II remains then metastable at ambient conditions. Commercial sample is instead a mixture of polymorphs I and II. The thermodynamic relationships between the two polymorphs were determined through the construction of an energy/temperature diagram. The *ab initio* structural determination performed on synchrotron X-Ray powder diffraction patterns recorded at RT on both polymorphs allowed us to elucidate, for the first time, their crystal structure. Both crystallize in the monoclinic space group type $P2_1/c$, and the unit cell similarity index and the volumetric isostructurality index indicate that the temperature-induced polymorphic transformation I→II is isostructural. Polymorphs I and II are conformational polymorphs, sharing a very similar hydrogen bond network, but with different conformation of the propanoic skeleton, which produces two different packing. The small conformational change agrees with the low value of transition enthalpy obtained by differential scanning calorimetry measurements and the small internal energy computed with density functional methods. © 2011 Wiley-Liss, Inc. and the American Pharmacists Association J Pharm Sci

Keywords: *ab initio* structural determination; carprofen; FTIR; MDSC; polymorphism; thermal analysis; X-ray powder diffractometry; crystal structure

INTRODUCTION

Active principles are known to often exist under different polymorphic modifications. The search for polymorphs and the characterization of their physicochemical properties has become a topic of major interest. Different molecular arrangements in the crystal lattice lead to considerable differences in solubility, bioavailability, stability, and technological behavior.[1,2] Therefore, the knowledge of the polymorphism of drugs is essential for the development of a successful pharmaceutical dosage form. Furthermore, regulatory agencies increasingly require detailed information and evidence of full control on polymorphism of drugs before allowing licensing and product distribution, making polymorphism screening of paramount importance during the formulation of a new drug.[1,3–4]

Carprofen [(*RS*)-2-(6-chloro-9*H*-carbazol-2-yl)propanoic acid] (Fig. 1) is a nonsteroidal anti-inflammatory drug used in veterinary medicine in the treatment of patients with rheumatoid arthritis, osteoarthritis, and acute gouty arthritis.[5–7]

Additional Supporting Information may be found in the online version of this article. Supporting Information

For structural investigations correspondence to: Fabia Gozzo (Telephone: +41-566-3103155; Fax: +41-56-3104551; E-mail: fabia.gozzo@psi.ch)

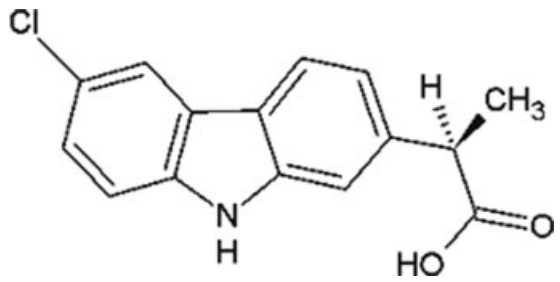

Figure 1. Structural formula of carprofen showing one of the two enantiomers present in the racemic compound analyzed.

Notwithstanding its use in the pharmaceutical industry, a deep physicochemical characterization of this active principle is still missing. In particular, the study of possible polymorphs and their structural characterization have, to the best of our knowledge, never been performed. The purpose of this work is a comprehensive characterization of the solid-state forms of carprofen to define both the thermodynamic relationships between its polymorphs through the construction of an energy/temperature diagram[8–10] and how this correlates with their crystal structures, as determined from powder diffraction (PD) data. The study has made use of conventional and innovative thermal techniques, Fourier-transform infrared (FTIR)spectroscopy, and laboratory and synchrotron radiation X-ray PD data (SR-XRPD).[11–20]

MATERIALS AND METHODS

All samples were obtained from the same commercial batch of carprofen (Sigma–Aldrich, Milan, Italy, batch no.: 8067x) with a stated purity of 99.9%. Measurements were performed on the commercial sample (*C* sample) and on samples recrystallized from hot solution of *C* sample in ethanol (*Re* sample), acetone, and isopropyl alcohol.

Among all recrystallized samples, only the one obtained from the ethanol solution showed significant and interesting differences with respect to the *C* sample. Therefore, the discussion is limited to the ethanol *Re* sample and the one obtained by heating of *Re* sample, denominated *HT-Re*. This study demonstrates that *Re* sample and *HT-Re* sample are two distinguished polymorphic forms of carprofen that we hereafter refer to as polymorph I (*Re* sample) and polymorph II (*HT-Re* sample).

Thermal analyses were carried out with a TGA Q5000 IR apparatus and a DSC Q2000 apparatus both interfaced with a TA 5000 data station (TA Instruments, New Castle, DE, USA). Thermogravimetric (TG) curves were recorded at 10 $K \cdot min^{-1}$, in a standard open platinum holder, under a nitrogen flow (3 $L \cdot h^{-1}$). The differential scanning calorimetry (DSC) instrument was calibrated using ultrapure (99.999%) indium (melting point, 156.6°C; ΔH = 28.54 $J \cdot g^{-1}$) as standard. The calorimetric measurements were conducted with open and closed standard aluminum pans under nitrogen flow (3 $L \cdot h^{-1}$) at different heating rate (2–120 $K \cdot min^{-1}$). All data derived from thermal measurements are the average of three or more experiments. DSC measurements with temperature modulation (MDSC) were performed with the same apparatus in closed pan at 3 $K \cdot min^{-1}$ (underlying heating rate) with period ranging from 30 to 100 s and temperature amplitude selected by the instrument according to the "heating only" mode (no cooling of the sample during temperature modulation).

Laboratory X-ray diffraction measurements (Ni-filtered CuK_α radiation; voltage of 40 kV and current of 30 mA) were performed using a D5005 Bruker powder diffractometer (Siemens, Karlsruhe, Germany) equipped with a θ–θ vertical goniometer and a position sensitive detector (PSD; MBraun, Garching, Germany). The patterns were recorded at room temperature (RT) in step scan mode (step size: 0.015°, counting time: 0.5 second per step) in the $5 < 2\theta^\circ < 40$ angular range. SR-XRPD measurements were performed at the Swiss Light Source (SLS) Materials Science (MS) beamline PD station. All samples were mounted in 0.8 mm Lindemann capillaries spinning at 10 Hz and measured at RT and at 150 K in Debye–Scherrer (transmission) geometry at nominal 0.8 Å using the one-dimensional MYTHEN silicon solid-state high-resolution detector.[21] For the low temperature SR-XRPD measurements, we made use of an Oxford cryojet (Oxford Instruments, Oxfordshire, UK). Whole PD patterns over 120° in 2θ were collected from the three carprofen powders (C, polymorphs I and II) for 10 s. The extremely high efficiency of MYTHEN detector allowed us to record statistics of the order of 90,000 counts per second in very short acquisition times (10 s) and avoid, therefore, sample radiation damage that is often observed when using synchrotron radiation for the analysis of organic materials.[22] The working photon wavelength and the 2θ zero offset were carefully calibrated by recording the diffraction pattern from a silicon standard (NIST 640C) and performing a Le Bail refinement with an *in-house* refinement program optimized for the MS-PD beamline optics and detectors. The result of the silicon refinement has given for the wavelenght of 0.799980 ± 0.000131 Å. Indexing of the SR-XRPD diffraction patterns was performed using EXPO2009 program.[23] Pawley refinement, structure solution, and Rietveld refinement were, instead, performed using TOPAS V3.0 software (Bruker AXS, Karlsruhe, Germany).[24] A model of the carprofen molecule was generated, using density functional theory (DFT) in the gas phase (*vide infra*). This model

was used to carry out direct-space searches of the crystal structure, using a simulating annealing technique. Trial structures are generated independently on the experimental data, by moving the molecular structure within the identified unit cell and according to its space group symmetry.[25,26] The model geometry was maintained rigid, but for the conformation of the flexible propanoic part, which in fact resulted quite fundamental. The suitability of each generated trial structure was assessed by direct comparison with the experimental diffraction data and quantified by the R_{wp}-factor and Goodness-of-Fit (GoF) statistical indicators, as defined in literature.[27]

Both the Pawley refinement and the simulating annealing were performed over a 2θ range from 2° to 40°. For the simulating annealing, the adopted temperature regime generates four to six moves per Marquardt Cycle (MC). For polymorph I, a plausible structural solution model was found after approximately 700 moves (95 MC) and reproduced every 500–700 moves (65–95 MCs), whereas for polymorph II, after approximately 1200 moves (130 MC) and reproduced every 1000–1200 moves (110–130 MCs).

For both polymorphs I and II, the Rietveld refinement was performed over a 2θ range of 2° to 45°, being both diffraction patterns essentially structureless above 45°. Extending the interval of the Rietveld refinement up to 65° reduces the value of R_{wp} and GoF but considerably slows down the computational time without affecting the result of the refinement.

During the Rietveld refinement, for both polymorphs I and II, the isotropic thermal parameters (B_{iso}) of all non-H atoms were refined, whereas the H atoms B_{iso} were kept at a fixed value of 4 Å^2. The phenyl ring carbon atoms were constrained to the same value, whereas all other non-H atoms were left free to vary independently on one another. A total number of 111 and 85 parameters were refined in the final Rietveld refinement for polymorphs I and II, respectively, which include the parameters refined to correct for microstructure effects, as discussed later.

FTIR spectra by diffuse reflectance were obtained with a Nicolet FT-IR 730 spectrometer (Nicolet, Madison, WI, USA) equipped with a DRIFT collector by Spectra Tech (Shelton, CT, USA). Samples were thoroughly mixed with anhydrous KBr, and the spectra were collected by coadding 1024 scans in the 4000 to 400 cm^{-1} range at 4 cm^{-1} resolution.

Gas phase DFT calculations were carried out on the carprofen isolated molecule using Gaussian09[28] at B3LYP/6–311G(2d,2p) level of theory, in order to obtain an accurate molecular geometry to be used in the rigid body refinement of the powder X-ray diffraction data. Solid-state calculations, with periodic boundary conditions, were also carried out on both polymorphs I and II, in order to confirm the presence of two distinct stationary points on the potential energy surface and to estimate their different energies. Because of the large size of the molecule and the relatively large number of atoms in the unit cell, these calculations were carried out with the following conditions: (a) only the two polymorphs have been investigated and no further search was made to find other possible polymorphs, (b) calculations were carried out at 0 K only, (c) the hybrid functional B3LYP was used, with a 6–21(d) basis set for C, N, O; 3–21(p) for H and 6–21 large core effective potential for Cl atoms (using 3-1 split for the valence orbitals). Periodic DFT calculations were carried out using CRYSTAL09.[29]

RESULTS AND DISCUSSION

Thermal Measurements

Commercial Sample

The TG analysis shows that the *C* sample does not contain any residual solvent. DSC cyclic measurements were carried out, in open and closed aluminum pans, at various heating rates β, ranging from 0.5 to 30 K·min^{-1}. The DSC curve recorded during the first heating cycle (Fig. 2a) shows only an endothermic peak of melting. Its onset temperature and enthalpy change do not depend on heating rate and on pan configuration (open or closed): $T_C = 211.8 \pm 0.4^\circ$C; $\Delta H_C = 112.3 \pm 1.4$ J·g^{-1}. During cooling down to RT, an exothermic peak is present due to the sample crystallization (Fig. 2b) while the second run quantitatively and qualitatively matches the first one (Fig. 2c).

Recrystallized Samples

According to the TG analysis, the *Re* sample (polymorph I) does not contain any residual solvent; the calorimetric behavior is reported in Figure 3. The DSC curve at 10 K·min^{-1} rate shows two endothermic peaks: a weak and broad peak in the temperature range 155°C–200°C (see inset in Fig. 3) followed by a sharp one at $212.3 \pm 0.2^\circ$C, corresponding to the melting temperature of the *C* sample. Because TG measurements indicate that the new endothermic effect is not associated to a mass change, we suppose it is due to a solid–solid transition, that is, to a polymorphic transformation. Experimentally, we observed that the parameters of transition peak are independent of the pan configuration while they depend on the heating rate as reported in Table 1. In particular: the onset temperature gradually increases with increasing β; the enthalpy change is constant at $\Delta H_t = 15.8 \pm 0.40$ J·g^{-1} with $\beta \leq 10$ K·min^{-1}. At heating rates >10 K/min^{-1}, the transition and melting peaks are not well separated, so that a reliable integration of them cannot be performed. However, the total integration of these two partially overlapping effects agrees, within the experimental error, with the

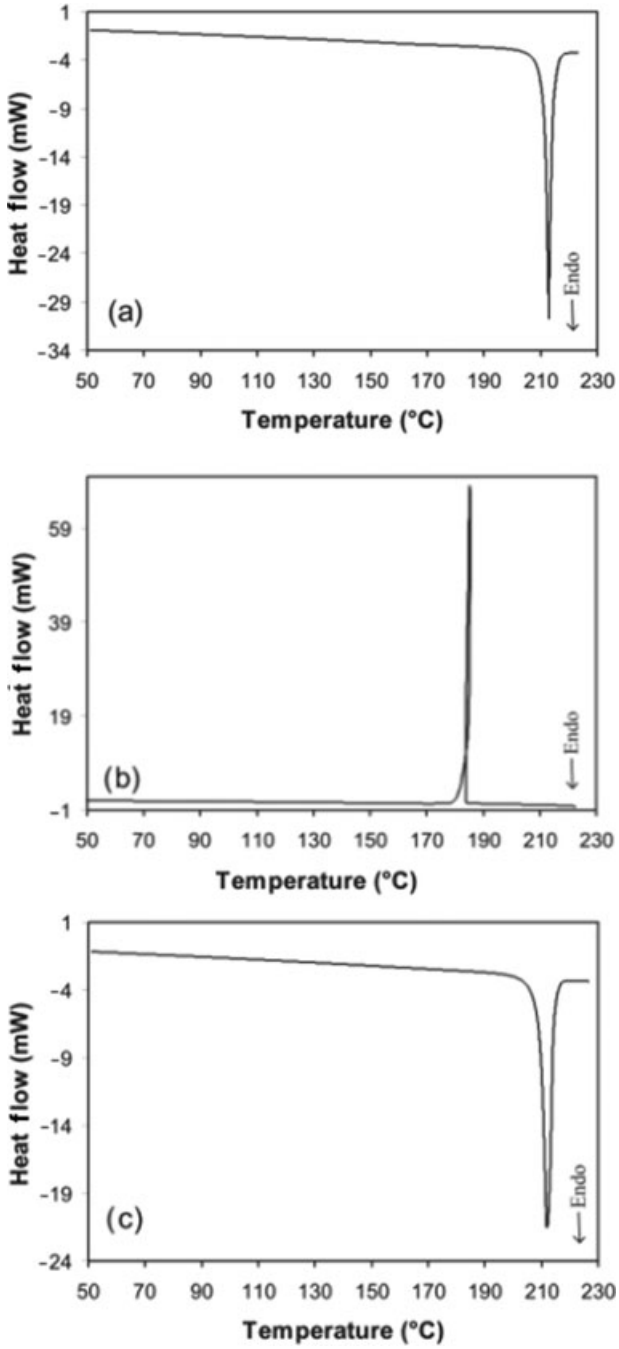

Figure 2. DSC curves of the *C* sample in closed pan at 10 K·min^{-1}: first heating (curve a), cooling (curve b) and second heating (curve c).

sum of the enthalpy values separately measured for the two peaks at $\beta \leq 10$ K·min^{-1}.

The thermal behavior of the *Re* sample (polymorph I) during cooling and second heating is similar to that of *C* sample. If the sample is heated up to the end of the transition peak (for example, to 198°C with $\beta = 2$ K·min^{-1} or to 203°C with $\beta = 10$ K·min^{-1}), so to prevent the occurrence of melting, no thermal event is recorded during subsequent cooling. The resultant

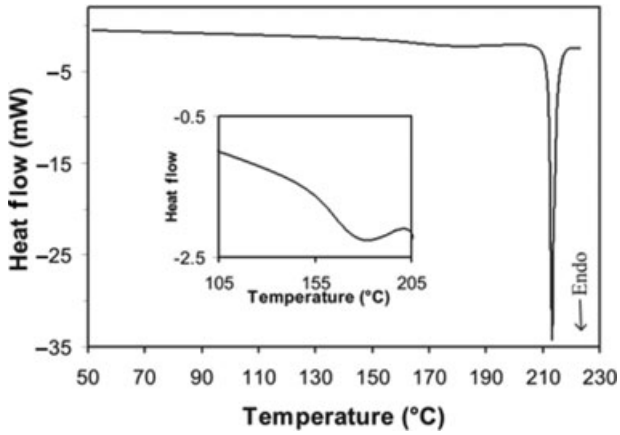

Figure 3. DSC curve in closed pan at 10 K·min^{-1} of the *Re* sample; in the inset the enlarged view of the endothermic peak is shown.

sample is characterized by a DSC curve that overlaps with that of the as-purchased *C* sample and is the one denominated *HT-Re* sample (polymorph II). The transition peak is thus not reversible, at least within the time scale of the measurements.

Isothermal Measurements

In order to better characterize the phenomenon at the origin of the transition peak, DSC measurements at 10 K·min^{-1} in closed pan were performed with an isothermal step inserted in the dynamic run at different temperatures below the onset temperature of the transition peak. As it can be seen in Figure 4, the enthalpy of the transition does not change significantly after 6 h annealing at 140°C. In contrast, with increasing isothermal temperature and time, it appreciably decreases. In particular, when the isothermal temperature increases, the reduction of the transition peak area emphasized with lower annealing time. After 30 h at 155°C, the transition peak vanishes. On the contrary, within the experimental error, the annealing does not affect the melting enthalpy.

Table 1. Quantitative Data Obtained for the *Re* Sample Transition Peak (T_t and ΔH_t are the Onset Temperature and the Enthalpy Change; ΔH_{t+C} is the Total Enthalpy Change of Both Transition and Melting)

β (K·min^{-1})	T_t (°C)	ΔH_t (J·g^{-1})	ΔH_{t+C} (J·g^{-1})
2	149.0 ± 0.3	16.0 ± 0.4	127.4 ± 0.5
5	150.7 ± 0.2	15.4 ± 0.6	128.0 ± 0.4
10	155.7 ± 0.3	15.8 ± 0.5	128.2 ± 0.3
20	156.4 ± 0.5	–	127.9 ± 0.4[a]
30	159.6 ± 0.6	–	126.7 ± 0.6[a]
40	162.5 ± 0.6	–	126.2 ± 1.2[a]
60	164.1 ± 0.4	–	127.8 ± 0.7[a]
80	166.3 ± 0.4	–	128.2 ± 1.1[a]
100	168.9 ± 0.3	–	128.9 ± 0.7[a]
120	170.1 ± 0.2	–	128.7 ± 1.1[a]

[a] Unsatisfactory to allow the integration of the single effects.

DOI 10.1002/jps

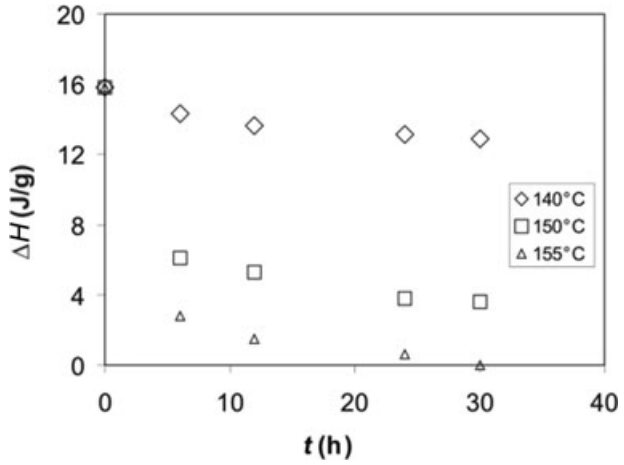

Figure 4. The transition enthalpy as a function of the isothermal temperature and time.

Thus, the measurements with the isothermal step show that the phenomenon at the origin of the broad peak can take place also at temperatures lower than in dynamic runs. This behavior is usually observed in kinetically driven transitions.

DSC Measurements with Temperature Modulation

Further information about the phenomenon marked by the broad DSC peak can be deduced by the MDSC technique, which through the application of a sinusoidal heating program on the sample, allows us to define the reversing (that can reverse over the time scale of the modulation) and nonreversing character (that depends only on time and kinetics processes) of the thermal events. In Table 2, it can be observed that, for all modulation periods chosen at the underlying heating rate of 3 $K \cdot min^{-1}$, the transition enthalpy measured from the total heat flow curve (ΔH_{Tot}), overlapping a conventional DSC curve, well agrees with the enthalpy value obtained from the not reversible heat flow curve (ΔH_{NotRev}). Thus, the MDSC measurements confirm the kinetic character, which is at the origin of the transition peak.

Table 2. Enthalpy Values from the Total Heat Flow (ΔH_{Tot}) and from the Nonreversible Heat Flow (ΔH_{NotRev}) Measured for the Sample Recrystallized from Ethanol at Different Periods/Temperature Amplitudes (Underlying Heating Rate: 3 $K \cdot min^{-1}$)

P (s)	A (°C)	ΔH_{Tot} ($J \cdot g^{-1}$)	ΔH_{NotRev} ($J \cdot g^{-1}$)
30	±0.24	15.5	15.4
40	±0.32	15.4	15.8
50	±0.40	15.2	15.1
60	±0.48	15.2	15.0
70	±0.56	15.3	15.1
80	±0.64	15.6	15.4
90	±0.72	15.0	14.7
100	±0.80	15.7	14.9
		15.3 ± 0.2	15.2 ± 0.3

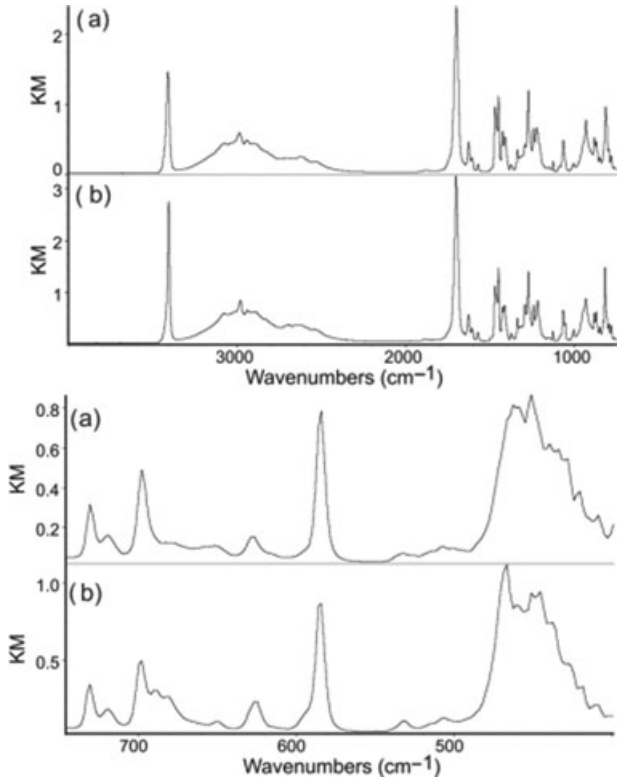

Figure 5. FTIR spectra and their enlarged view, of *C* (a) and *Re* (b) samples.

FTIR Measurements

The FTIR spectrum reported in Figure 5a is characteristic of both the *C* sample and the *HT-Re* sample. In Table 3, the assignment of various peaks are reported. The FTIR spectrum of *Re* sample (Fig. 5b) looks very similar to the *C* sample. The only difference is the presence of two additional peaks in the region of 690 to 670 cm^{-1} (see Figs. 5a and Figs. 5b, enlarged view).

Table 3. Wavenumbers (cm^{-1}) of the FTIR Spectra of *C* Sample

Wavenumbers (cm^{-1})	Assignments
3410	NH stretching
Broad band 3300 to 2400	OH stretching
1701	C═O stretching
1627; 1572; 1471; 1427; 1337	Aromatic ring stretching (di-light, heavy)
1450	OH in plane deformation
1411	NH in plane deformation
1273	Combination of C—O stretching and OH deformation
1222	CN stretching
1241; 1126; 1065	Aromatic CH in plane deformation
930	OH out of plane deformation
1004; 880–869; 813	Aromatic CH out-of-plane deformation
730	NH wagging
627	C═O out-of-plane deformation
697; 584; 468	Aromatic ring out-of-plane deformation

XRPD Measurements

Laboratory XRPD

The *C* sample *C* as well as polymorphs I and II powders were first inspected using laboratory XRPD. All powder patterns were recorded at RT. Polymorph II was characterized by reflections considerably sharper than polymorph I, indicating a higher degree of crystallinity. Besides these microstructural features, the diffraction patterns of polymorphs I and II showed significant differences in peaks positions and diffracted intensities and confirmed the occurrence of a polymorphic transformation, as already suggested by thermal measurements.

The XRPD pattern of *C* sample shows a degree of crystallinity similar to polymorph I and a comparison with the powder patterns of polymorphs I and II suggested *C* sample being a mixture of these two phases. Laboratory XRPD data did not allow conclusive structural analyses and, therefore, for the *ab initio* structural solution and refinement, SR-XRPD measurements were performed at RT and at 150 K. Figure 6 shows for a direct comparison the SR-XRPD patterns of the *Re*, *HT-Re*, and *C* powder samples. Figure 7 shows the atoms numbering used for the structural investigation and the torsion angles for the carprofen molecule.

Ab Initio SR-XRPD Structure Determination

Crystallographic data of polymorphs I and II are reported in Table 4. [1] Both crystallize in the monoclinic space group type $P2_1/c$. The low unit cell similarity index ($\Pi = 0.00177$) and the high volumetric isostructurality index ($I_v = 66.7\%$) indicate that the temperature-induced polymorphic transformation I→II is isostructural.[30] The crystal packing of the two polymorphs, therefore, does not change but the lattice parameters and unit cell volumes undergo small but statistically significant variations: $\Delta a/a \sim +3.3\%$, $\Delta b/b \sim +1.5\%$, $\Delta c/c \sim -1.1\%$ with β changing by $\sim 3.6^\circ$ and a unit cell volume expansion of $\Delta V/V \sim +2.6\%$. No indexation was possible for *C* sample; however, this powder pattern is compatible with a mixture of the two phases (see below).

Structure Determination of Polymorphs I and II

The SR-XRPD pattern of polymorph I was indexed with a monoclinic cell ($a = 27.13$ Å, $b = 5.71$ Å, $c = 8.29$ Å, $\beta = 96.92^\circ$; $M_{20} = 13$,[31] no unindexed lines) by EXPO2009[23] using 17 peaks in the first 20° in 2θ. Systematic absences indicated the symmetry of the space group $P2_1/a$ (no. 14) type with a Figure-of-Merit of 0.51.[32–34] Similarly, using 15 peaks in the first 20° in 2θ, the SR-XRPD pattern of polymorph II was indexed with a monoclinic cell ($a = 26.59$ Å, $b = 5.79$ Å, $c = 8.55$ Å, $\beta = 97.97^\circ$; $M_{20} = 22$, no unindexed lines) in the space group $P2_1/n$ (no. 14) type with a Figure-of-Merit of 0.55. A simple cell transformation brought $P2_1/a$ and $P2_1/n$ to the standard $P2_1/c$ representation.

For both polymorphs I and II, the most appropriate analytical functions for the peak line shapes (Thompson–Cox–Hastings Pseudo-Voigt function convoluted with the Finger–Cox–Jephcoat asymmetric function)[35,36] and the background (20th degree polynomial function), as well as the 2θ-scale zero error and the cell parameters were determined by performing a whole pattern Pawley refinement.

A rigid body was constructed based on the DFT calculated gas phase molecular structure and used for the simulating annealing search of both polymorphs I and II of carprofen. Only the C—O and C=O distances of the carboxylic group were adjusted to the experimental interatomic distances, as provided by the

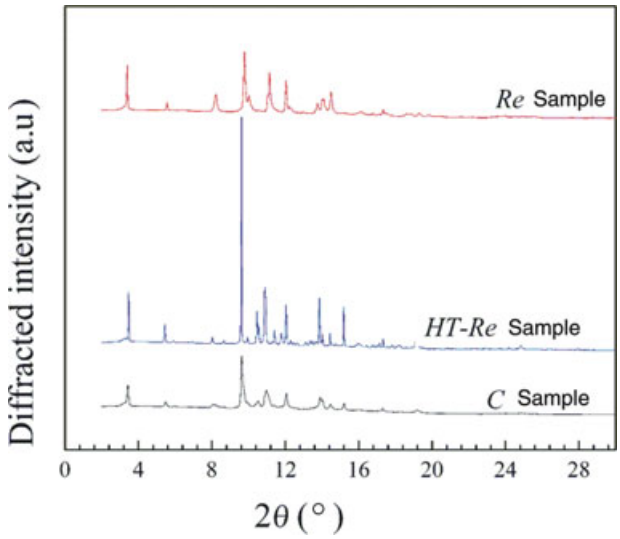

Figure 6. SR-XRPD patterns of (a) *Re*, (b) *HT-Re*, and (c) *C* samples.

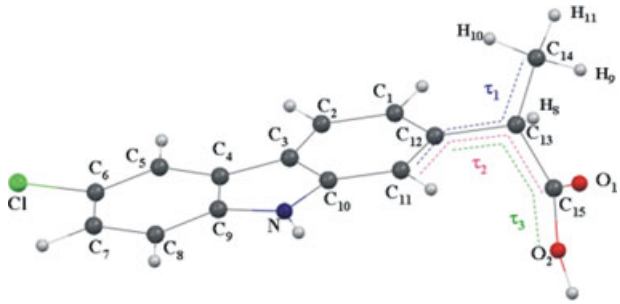

Figure 7. Three-dimensional molecular structure of carprofen showing the torsion angles τ_1, τ_2 and τ_3 that significantly change from polymorph I to II, as discussed in the text.

[1] CCDC 779551 and 779552 (RT structure) and CCDC 798188 and 798189 (150 K structure) contain the supplementary crystallographic data for this paper. These data can be obtained free of charge via www.ccdc.cam.ac.uk/data_request/cif.

Table 4. Crystallographic Data of Polymorphs I and II of Carprofen at Room and Low Temperature from SR-XRPD and from DFT Calculations (0 K Simulation)

	SR-XRPD	SR-XRPD	SR-XRPD	SR-XRPD	DFT	DFT
Polymorph	I	II	I	II	I	II
Temperature (K)	298	298	150	150	0	0
Empirical formula	$C_{15}H_{12}ClNO_2$	$C_{15}H_{12}ClNO_2$	$C_{15}H_{12}ClNO_2$	$C_{15}H_{12}ClNO_2$	$C_{15}H_{12}ClNO_2$	$C_{15}H_{12}ClNO_2$
Formula weight	273.72	273.72	273.72	273.72	273.72	273.72
Crystal system	Monoclinic	Monoclinic	Monoclinic	Monoclinic	Monoclinic	Monoclinic
Space group type	$P2_1/c$ (n.14)	$P2_1/c$ (n.14)	$P2_1/c$ (n.14)	$P2_1/c$ (n.14)	$P2_1/c$ (n.14)	$P2_1/c$ (n.14)
A [Å]	8.2855 (3)	8.5563(3)	8.2210 (3)	8.5084 (2)	8.23	9.16
b [Å]	5.7071 (3)	5.7923 (2)	5.6650 (3)	5.7415 (2)	5.55	5.44
c [Å]	27.087 (1)	26.778 (1)	26.937 (1)	26.573 (1)	26.84	26.07
β [°]	96.901 (5)	100.473 (3)	96.942 (4)	100.579 (3)	101.0	110.1
V_{cell} [Å^3]	1271.57(10)	1305.05(8)	1245.3(1)	1276.05 (8)	1204	1220.
Z	4	4	4	4	4	4
Calculated density (g/cm^3)	1.43	1.40	1.46	1.425	1.51	1.49
R_{wp}[a] (%); GoF[a] (Pawley)	2.25; 3.26	2.16; 3.63	–	–		
R_{wp} (%); GoF (Simulating annealing)	7.09; 11.76	6.41; 10.30	–	–		
R_{wp}(%); GoF (Rietveld refinement)	1.77; 2.85	2.09; 3.26	1.96; 3.21	2.60; 4.06		

[a]The R-weighted pattern (R_{wp}) and the Goodness-of-Fit (GoF) statistical indicators are defined in Ref. 27.

International Tables for Crystallografy (ITC),[37] which take into account the perturbation of the intermolecular hydrogen (H) bonding, occurring in both the solid-state forms [C—O of 1.305 Å instead of 1.355 Å of the free molecule and C=O (1.214 Å) instead of 1.204 Å of the free molecule]. During the simulating annealing search and the subsequent Rietveld refinement, bond lengths and angles were constrained to the values defined by the calculated molecular structure, whereas the trial structure was assigned two internal (torsions) and six external degrees of freedom, the latter corresponding to the overall translation and rotation of the molecule (see Fig. 7). No restraints were applied to the internal and external degrees of freedom. The additional two internal degrees of freedom (torsions around C_{15}-OH and C_{13}-CH_3) were not varied during the simulating annealing search being XRPD insensitive to the position of H atoms.

The successful result of structure solution was, then, refined by a subsequent Rietveld refinement. (Fig. 8). The graphical inspection of the Rietveld refinement of both polymorphs I and II indicated the presence of anisotropic hkl (Miller indices)-dependent peak broadening, which was successfully corrected using a phenomenological model developed by Stephens in 1999 based on a multidimensional distribution of lattice metrics within the powder sample, and implemented in Topas.[38] In addition to anisotropic peak broadening, the SR-XRPD pattern of polymorphs I and II were also corrected for preferential orientation using a model based on spherical harmonics and implemented in Topas.[24]

During the refinements, the B_{iso} of the methyl group carbon atom and to a less extent of the oxygen atoms of the carboxylic group converged for polymorph II toward values higher than expected. In particular, the methyl group carbon atom (C14)

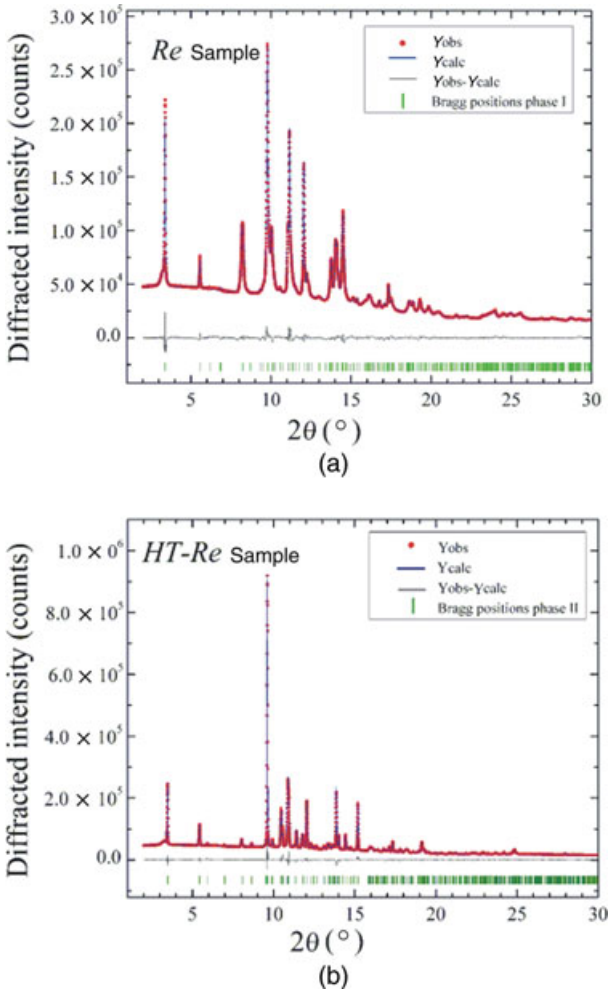

Figure 8. Rietveld refinement for polymorphs I (a) and II (b), which shows the simulated y_{calc} SR-XRPD pattern (solid blue line), the experimental SR-XRPD pattern y_{obs} (red crosses), their difference $y_{obs} - y_{calc}$ (solid gray line), and the expected Bragg reflections (green bars).

converged to a value of B_{iso} higher than 60 Å^2. This may reasonably indicate the presence of some sort of crystallographic disorder, which is not solved even by analyzing SR-XRPD recorded at low temperature (150 K), as B_{iso} of C14 converges instead toward an even larger value. A conformational disorder about C12—C13 and C13—C15 was tentatively refined, but it gave inconsistent geometries.

We considered, therefore, the possibility of configurational disorder, assuming that at each molecular site both enantiomers are present. This hypothesis basically corresponds to a disorder between the methyl group C14 and the H8 atom and was indeed successfully refined returning an occupation ratio of approximately 70%:30% for polymorph II with a reduced B_{iso} value and an improved refinement. An equivalent disorder analysis conducted on polymorph I returned an occupation ratio of approximately 90%:10%, value reasonably close to the limit of the accuracy with which such an analysis of disorder can be conducted even using high-resolution SR-XRPD. Table S.I.1 and S.I.2 in the Supplementary Information summarize the relevant bond lengths and torsions as well as the thermal parameters for polymorphs I (Table S.I.1) and II (Table S.I.2). Figures 9a and Figures 10a show the molecular packing generated using only the predominant configurations, whereas Figures 9b and Figures 10b show superposition of both the major and minor configurations of polymorphs I and II, respectively. It appears that the volume increase that characterizes polymorph II allows the accommodation of both configurations in the molecular packing. In polymorph I, instead, the alternative configuration is quite hindered and it would imply an unfavorable Cl— C14 distances (<3 Å). Noteworthy for both polymorphs the disorder would not substantially change the supramolecular motif, which is dictated by the COOH groups and basically unaffected by the disorder.

An additional disorder could take place in the carboxylic group, due to a possible resonance between O=C—OH and HO—C=O configurations. This would affect mainly the two C— O distances, but any attempt to include this disorder resulted in unstable refinements. Nevertheless, the slightly higher B_{iso} obtained for the two oxygen atoms is in fact compatible with this kind of resonance disorder.

Commercial Sample. As already pointed out, a qualitative analysis of the XRPD pattern of *C* sample suggested that this sample could be a mixture of polymorphs I and II. The Rietveld refinement performed on the SR-XRPD data of *C* sample first with only the refined phase of polymorph I and, then, with both refined phases of polymorphs I and II clearly confirmed this hypothesis. The statistical indicators of the one-phase and the two-phases Rietveld refinement are $(R_{wp}, GoF)_{phase\ I} = 3.492, 5.633$ and $(R_{wp}, GoF)_{phase\ I + phase\ II} = 1.864, 3.010$. The contents of polymorphs I and II are 40 and 60 wt %.

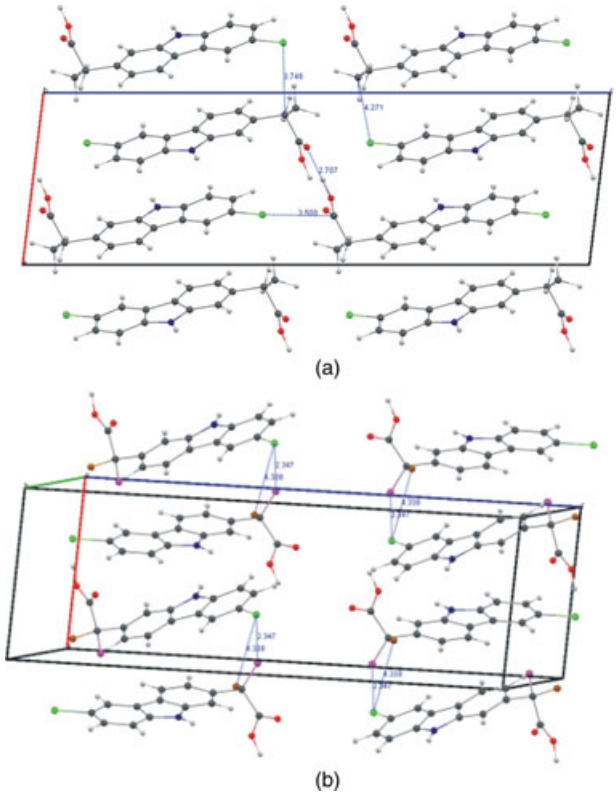

Figure 9. Molecular packing diagram of polymorph I showing the predominant configuration projected onto the b axis (a) and both the predominant (approximately 90%, C14 atom in brown) and the disordered (approximately10%, C14 atom in magenta) configurations (b).

Figure 11 shows the plot of the multiphase Rietveld refinement of *C* sample, the residuals of the refinement and the expected Bragg positions for both components I and II.

DISCUSSION

Both thermal and crystallographic investigations suggest that *Re* and *HT-Re* samples are different polymorphic forms of carprofen. Polymorphic transformations that do not imply a dramatic change of the unit cell parameters and the crystal symmetry but are only associated with topographically different (or differently oriented) H bonds and different intermolecular interactions induced by variations of torsion angles, although uncommon, are known in literature.[39,40] Polymorphism should, however, in such cases be assessed with particular caution, especially when polymorphic studies are conducted in nonambient conditions. Unusual anisotropic thermal expansions of the cell parameters have been, in fact, observed *in situ*

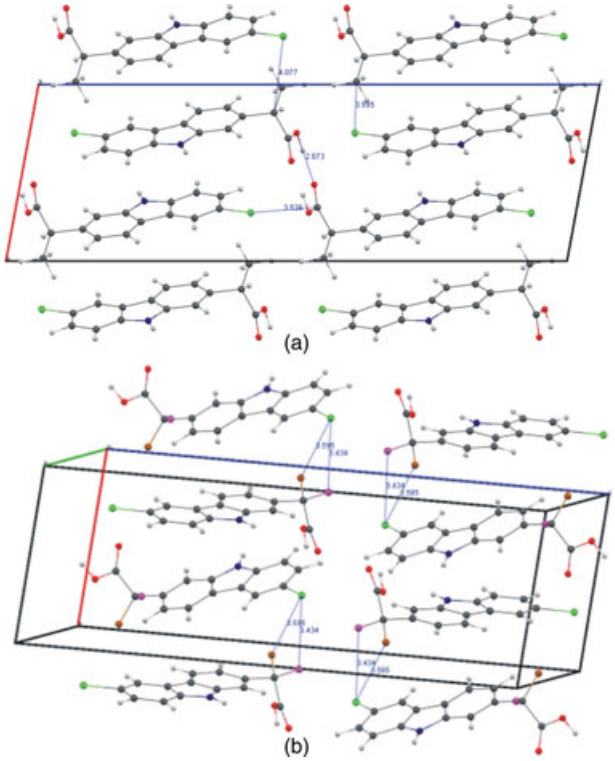

Figure 10. Molecular packing diagram of polymorph II showing the predominant configuration projected onto the b axis (a) and both the predominant (approximately 70%, C14 atom in brown) and the disordered (approximately 30%, C14 atom in magenta) configurations (b).

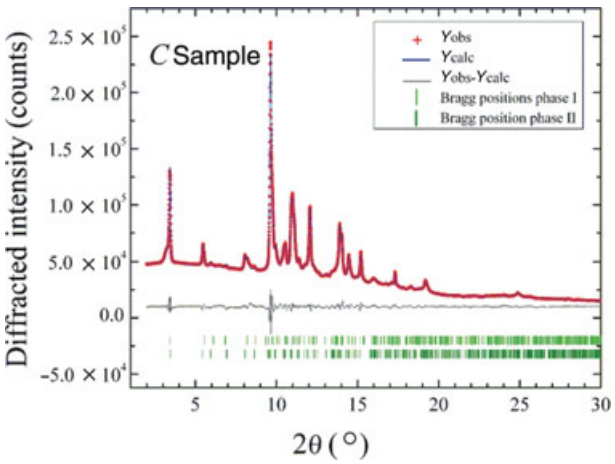

Figure 11. Rietveld refinement of *C* sample SR-XRPD pattern showing the simulated y_{calc} SR-XRPD pattern (solid blue line), the experimental y_{obs} SR-XRPD pattern (red crosses), their difference $y_{obs} - y_{calc}$ (solid gray line), and the expected Bragg reflections (light green bars: phase I, dark green bars: phase II).

as a function of temperature, which were intricate to clearly distinguish from isostructural conformational polymorphism.[41,42]

The Rietveld analysis performed on high-resolution SR-XRPD data of the as-purchased *C* sample ascertained, on the other hand, that the sample is a mixture of polymorphs I and II, although with low crystallinity. This result was, however, not conclusively confirmed by DSC measurements due to the very low transition enthalpy characterizing polymorph I that, at fractions of only 40 wt %, falls below the sensibility of the DSC technique.

On the basis of the *heat of fusion rule*[8] according to which the highest melting form is enantiotropically related to the other form, if it shows the lowest enthalpy of fusion, the relative thermodynamic stabilities of the polymorphic pairs are determined. In our case, the melting point of polymorph I cannot be directly measured. However, because an endothermic transition peak is recorded during its heating, an enantiotropic relationship must necessarily exist between forms I and II,[8] and the melting onset temperature of polymorph I must inevitably be lower than the one characterizing polymorph II. Polymorph I is, therefore, the RT stable form of carprofen.

According to Hess's law of heat summation, the melting enthalpy of polymorph I can be derived as the sum of the melting enthalpy of polymorph II and the transition enthalpy:

$$\Delta H_{\mathrm{I}} = \Delta H_{\mathrm{t}} + \Delta H_{\mathrm{II}} = 15.8 + 112.3\mathrm{J}^{-1} = 128.1\mathrm{J}^{-1}$$

The melting onset temperature of polymorph I can, then, be estimated by applying the thermodynamic model of Burger and Ramberger to our data expressed by the following equation[8–10]:

$$T_{\mathrm{t}} = \frac{\left[\Delta H_{\mathrm{II}} - \Delta H_{\mathrm{I}} + 0.003 \cdot \Delta H_{\mathrm{I}} \cdot (T_{\mathrm{I}} - T_{\mathrm{II}})\right]}{\frac{\Delta H_{\mathrm{II}}}{T_{\mathrm{II}}} - \frac{\Delta H_{\mathrm{I}}}{T_{\mathrm{I}}} + 0.003 \cdot \Delta H_{\mathrm{I}} \cdot \ln \frac{T_{\mathrm{I}}}{T_{\mathrm{II}}}} \qquad (1)$$

modified as in reference[10]:

$$T_{\mathrm{I}} = \frac{\Delta H_{\mathrm{I}} T_{\mathrm{II}} T_{\mathrm{t}}}{T_{\mathrm{II}} \Delta H_{\mathrm{I}} + T_{\mathrm{t}} \Delta H_{\mathrm{I1}} - T_{\mathrm{II}} \Delta H_{\mathrm{I1}}} \qquad (2)$$

For the melting onset temperature of polymorph I, we, then, obtain: $T_{\mathrm{I}} = 203.1^{\circ}\mathrm{C}$, which is, as expected, located between the transition temperature and the melting temperature of the highest melting point polymorph (form II).

The small enthalpy variation of the transition peak (ΔHt) and the similarities of forms I and II FTIR spectra are completely consistent with our crystallographic structural observations. Polymorphs I and II are, in fact, related by an isostructural transformation with small but significant unit cell volumes and cell parameters variations, due to a conformational rearrangement. Although we could not measure the PD patterns at the critical temperature, all other data suggest that the transformation is compatible with a first-order phase transition, taking also into account

the metastability of polymorph II once cooled at ambient conditions.

The main difference between polymorphs I and II is the rotation of the propane skeleton about the C_{12}-C_{13} bond (i.e., the connection to the carbazolyl ring). Following Klyne and Prelog's[43] nomenclature and assuming the Cl atom as the reference for the carbazolyl ring and the COOH for the propanoic skeleton, polymorph I has an *anticlinal* conformation whereas polymorph II has a *synclinal* conformation (though very close to a 90° torsion). Thus, because the carboxylic groups have a different orientation with respect to the condensed ring, the two different supramolecular motifs are generated through strong H-bound dimerization, as shown in Figure 12.

In the gas phase, the most stable conformation is also *synclinal*, like in polymorph II, but the H8 atom is *anti* instead of *syn*. It is clear that rotation about the C_{12}-C_{13} bond is quite easy and several conformations could in principle be possible.

The structural analysis suggests that with temperature, the increased energy of the system allows torsions τ_1 (methyl group), τ_2 and τ_3 (carboxylic group) to sensibly change while the unit cell undergoes a volumetric thermal expansion. When the orientation of the flexible fragments is such that a shorter length along c is sufficient to accommodate the methyl and carboxylic groups (see Figs. 9 and 10), the c-axis shrinks and makes the ongoing thermal expansion anisotropic. The contraction of the c-axis of polymorph II allows the H bonds of the centrosymmetric

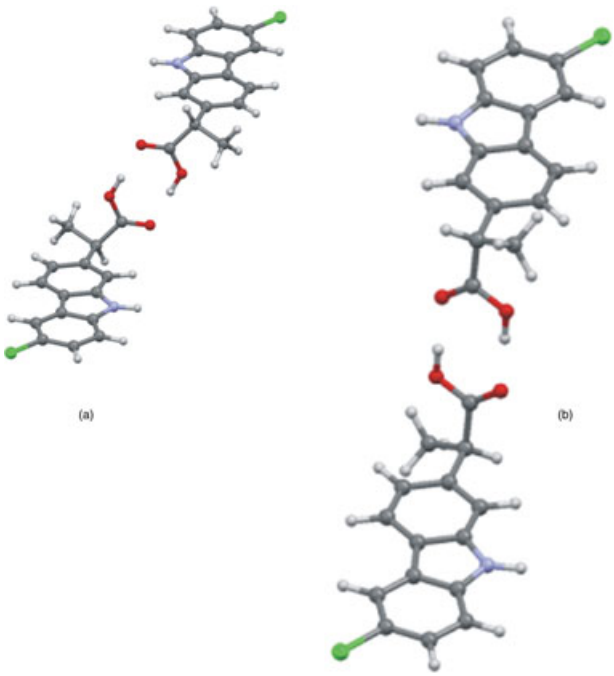

Figure 12. The hydrogen-bonded dimer in polymorphs I (a) and II (b).

– C···O···H– – –O=C– dimers to maintain a reasonable value in spite of the elongation of *a* and *b* cell parameters due to the increase of temperature.

The significant variation of the molecular internal degrees of freedom (in particular τ_3) changes the H-bonded interactions between Cl and C atoms.

The averaged H bond interaction between the N atom and the C atoms of the Cl–phenyl group (N– – – phenyl ring) that holds together the carbazole[44] rigid fragments of carprofen only slightly changes for polymorphs I and II (Å average value of <3.58> for polymorph I and <3.68> for polymorph II) confirming, indeed, that the polymorphic transformation only involves the rearrangement of the orientation of the flexible fragments of carprofen.

XRPD measurements of form II at RT several weeks after the preparation confirm the presence of this polymorph without any evidence of transformation to polymorph I. This is consistent with the structural analysis results of the *C* sample, containing both forms of carprofen. The mechanism behind could be that the modified H bond interactions in polymorph II that follow the variation of the molecular internal degrees of freedom induced by temperature are *locked* by the shrinking of the unit cell c-axis that makes, therefore, the transformation not reversible upon cooling.

The DFT geometries confirm the two conformations and packing motifs, but they disagree with the experiments in the unit cell constants, especially the β angles (see Table S.I.1 and S.I.2).

The potential energy surface of polymorph II is also more difficult to investigate being it lacks of a deep minimum. Furthermore, the presence of configurational disorder in the two structures (especially polymorph II) does not allow us to compare the calculated energies with enthalpies measured with DSC. Nevertheless, all calculations indicate that polymorph I is associated with a lower internal energy. This is also consistent with the shorter –C···O···H– – –O=C–, Cl– – $-C_{13}$ and Cl– – $-C_{14}$ bonds of form I with respect to Form II and confirm that form II is, indeed, a less stable form of carprofen. Because the transformation is associated with an endothermic peak, it must be induced a favorable entropic term, which is reasonable given by the larger volume of polymorph II.

Finally, structural investigations of *C* sample indicate that it is not a new polymorph of carprofen but a mixture of polymorphs I and II. The coexistence of polymorphs I and II in the *C* sample is not surprising because it is well known that processing methods during manufacturing of pharmaceuticals (grinding, milling, and tabletting) may induce phase changes in drugs. Significant localized compression and shear stresses, in addition to localized heating can, in fact, lead to the formation of new polymorphs.[45] The con-

 DOI 10.1002/jps

version of polymorph II back into I seems not to be favorable, at least at ambient conditions.

We also tried to induce II→I transformation by applying pressure up to 2.3 GPa, with the sample loaded in a gas membrane diamond anvil cell. Given the smaller volume of polymorph I, this transformation was expected to be favorable. However, we did not observe any phase change, but a progressive amorphization of the sample. Investigations on the recrystallization from solution under pressure are currently in progress (Simoncic P, et al. 2010, private communication).

CONCLUSIONS

Experimental evidences indicate that carprofen exist as two solid-state forms (polymorph I and polymorph II) in enantiotropic relationship. Polymorph I is the stable phase at RT, but it transforms upon heating into polymorph II, which holds as a metastable form after cooling. Although being the melting point of polymorph I not directly measurable, the application of thermodynamic models to our data has allowed us to indirectly estimate its melting temperature and enthalpy change. High-resolution SR-XRPD data allowed us to elucidate the crystal structure of the two carprofen polymorphs. Both crystallize in the monoclinic space group type $P2_1/c$ and the unit cell similarity index and the volumetric isostructurality index indicate that the temperature-induced polymorphic transformation I→II is isostructural and due to a small conformational rearrangement. This agrees with the low value of transition enthalpy obtained by DSC measurements. The *C* sample is, on the contrary, a mixture of polymorphs I and II. The less stable form (polymorph II) appears to be characterized by a considerable configurational disorder that SR-XRPD data can assess as approximately in the ratio 70%:30%. Polymorph I might also be slightly affected by the same configurational disorder, but the poor crystallinity of these samples does not allow us to confirm it.

ACKNOWLEDGMENTS

These XRPD experiments were performed on the Materials Science beamline PD station at the Swiss Light Source, Paul Scherrer Institut, Villigen, Switzerland. P.M. and P.S. thank the Swiss National Science foundation (project 200021_126788/1). F.G. thanks the Paul Scherrer Institut Forschung Kommission (2010-2012 high-pressure crystallography on molecular crystals project). The authors are particularly grateful to Norberto Masciocchi for the fruitful discussions during the SR structural data analysis and to László Fábián and Alajos Kálmán for making the programs for the estimate of the unit cell similarity index and the volumetric isostructurality index kindly available and for the kind and generous help provided to operate the programs.

This article contains supplementary material available from the authors upon request or via the Internet at http://wileylibrary.com.

REFERENCES

1. Niederwanger V, Gozzo F, Griesser UJ. 2009. Characterization of four crystal polymorphs and a monohydrate of s-bupivacaine hydrochloride (levobupivacaine hydrochloride). J Pharm Sci 98:1064–1074.
2. Tedesco E, Giron D, Pfeiffer S. 2002. Crystal structure elucidation and morphology study of pharmaceuticals in development. CrystEngComm 4:393–400.
3. Vippagunta SR, Brittain HG, Grant DJW. 2001. Crystalline solids. Adv Drug Deliv Rev 48:3–26.
4. Hilfiker R, Blatter F, Raumer M. 2006. Relevance of solid-state properties for pharmaceutical products. In Polymorphism: in the pharmaceutical Industry. (Ed. R. Hilfiker), Wiley-VCH. Verlag GmbH & Co. KGaA, Weinheim, FRG, pp 1–19.
5. Yu TF, Perel J. 1980. Pharmacokinetic and clinical studies of carprofen in gout. J Clin Pharmacol 20:347–351.
6. Williams RL, Furst DE, Mandel HG, Nicoll D, Konikoff JJ, Benet LZ. 1981. Effects of indomethacin and carprofen on renal homeostasis in rheumatoid arthritis patients and in healthy individuals. J Clin Pharmacol 21:493–500.
7. O'Brien WM, Bagby GF. 1987. Carprofen: A new nonsteroidal anti-inflammatory drug. Pharmacology, clinical efficacy and adverse effects. Pharmacotherapy 7:16–24.
8. Burger A, Ramberger R. 1979. On the polymorphism of pharmaceutical and other molecular crystals. I. Theory of thermodynamic rules. Microchim Acta 11:259–271.
9. Yu L. 1995. Inferring thermodynamic stability relationship of polymorphs from melting data. J Pharm Sci 84:966–974.
10. Braun DE, Gelbrich T, Kahlenberg V, Tessadri R, Weiser J, Griesser UJ. 2009. Conformational polymorphism in aripiprazole: Preparation, stability and structure of five modifications. J Pharm Sci 98:2010–2026.
11. Giron D. 1995. Thermal analysis and calorimetric methods in the characterization of polymorphs and solvates. Thermochim Acta 248:1–59.
12. Gill PS, Sauerbrunn SR, Reading M. 1993. Modulated differential scanning calorimetry. J Therm Anal Calorim 40:931–939.
13. Coleman NJ, Craig DQM. 1996. Modulated temperature differential scanning calorimetry: A novel approach to pharmaceutical thermal analysis. Int J Pharm 135:13–29.
14. Marini A, Berbenni V, Bruni G, Sinistri C, Maggioni A, Orlandi A, Villa M. 2000. Physico-chemical characterization of a novel tricyclic beta -lactam antibiotic. J Pharm Sci 89:232–240.
15. Marini A, Berbenni V, Bruni G, Margheritis C, Orlandi A. 2001. Physico-chemical study of the solid forms of a new drug. J Pharm Sci 90:2131–2140.
16. Marini A, Berbenni V, Bruni G, Villa M, Orlandi A. 2002. Thermal decomposition and melting of a new carboxyindole derivative. J Therm Anal Calorim 68:389–396.
17. Bruni G, Berbenni V, Milanese C, Girella A, Cardini A, Viganò E, Lanfranconi S, Marini A. 2009. Thermodynamic relationships between nateglinide polymorphs. J Pharm Biomed Anal 50:764–770.
18. Bruni G, Berbenni V, Milanese C, Girella A, Cardini A, Lanfranconi S, Marini A. 2010. New modifications of nateglinide. J Pharm Biomed Anal 51:1054–1059.

19. Harris KDM. 2001. Structure determination of molecular crystals directly from powder diffraction data. Rigaku J 18:23–330.
20. Shankland K, Markvardsen AJ, David WIF. 2004. Powder diffraction based structural studies of pharmaceuticals. Z Kristallogr 219:857–865.
21. Bergamaschi A, Cervellino A, Dinapoli R, Gozzo F, Henrich B, Johnson I, Kraft P, Mozzanica A, Schmitt B, Shi X. 2010. The MYTHEN detector for XRPD experiments at the Swiss Light Source. J Synchrotron Radiat 17(5):653–668.
22. Holton JM. 2009. A beginner's guide to radiation damage. J Synchrotron Radiat 16:133–142.
23. Altomare A, Campi G, Cuocci C, Eriksson L, Giacovazzo C, Moliterni A, Rizzi R, Werner P-E. 2009. Advances in powder diffraction pattern indexing: N-TREOR09. J Appl Crystallogr 42:768–775.
24. Bruker AXS. 2000. TOPAS V3.0: General profile and structural analysis software for powder diffraction data. Karlsruhe, Germany: User Manual Bruker AXS.
25. David WIF, Shankland K, Shankland N. 1998. Routine determination of molecular structures from powder diffraction data. Chem Commun 8:931932
26. Tremayne M. 2004. The impact of powder diffraction on the structural characterization of organic crystalline materials. Philos Transact A Math Phys Eng Sci 362:2691–2707.
27. McCusker LB, Von Dreele RB, Cox DE, Louer D, Scardi P. 1999. Rietveld refinement guidelines. J Appl Crystallogr 32:36–50.
28. Frisch MJ, Trucks GW, Schlegel HB, Scuseria GE, Robb MA, Cheeseman JR, Scalmani G, Barone V, Mennucci B, Petersson GA, Nakatsuji H, Caricato M, Li X, Hratchian HP, Izmaylov AF, Bloino J, Zheng G, Sonnenberg JL, Hada M, Ehara M, Toyota K, Fukuda R, Hasegawa J, Ishida M, Nakajima T, Honda Y, Kitao O, Nakai H, Vreven T, Montgomery JA, Peralta JE, Ogliaro F, Bearpark M, Heyd JJ, Brothers E, Kudin KN, Staroverov VN, Kobayashi R, Normand J, Raghavachari K, Rendell A, Burant JC, Iyengar SS, Tomasi J, Cossi M, Rega N, Millam JM, Klene M, Knox JE, Cross JB, Bakken V, Adamo C, Jaramillo J, Gomperts R, Stratmann RE, Yazyev O, Austin AJ, Cammi R, Pomelli C, Ochterski JW, Martin RL, Morokuma K, Zakrzewski VG, Voth GA, Salvador P, Dannenberg JJ, Dapprich S, Daniels AD, Farkas O, Foresman JB, Ortiz JV, Cioslowski J, Fox DJ. 2009. Gaussian 09, Revision A.02, Gaussian, Inc., Wallingford, Connecticut..
29. Dovesi R, Saunders VR, Roetti C, Orlando R, Zicovich-Wilson CM, Pascale F, Civalleri BK, Doll K, Harrison NM, Bush IJ, D'arco P, Llunell M. CRYSTAL09 - CRYSTAL09 User's Manual, University of Torino, Torino, Italy, 2009.
30. Fabian L, Kalman A. 1999. Volumetric measure of isostructurality. Acta Crystallogr B 55:1099–1108.
31. Wolff, PM de. 1968. A simplified criterion for the reliability of a powder pattern indexing. J Appl Crystallogr 1:108–113.
32. Altomare A, Caliandro R, Camalli M, Cuocci C, da Silva I, Giacovazzo C, Moliterni AGG, Spagna R. 2004. Space group determination from powder diffraction data: A probabilistic approach. J Appl Crystallogr 37:957–966.
33. Altomare A, Camalli M, Cuocci C, da Silva I, Giacovazzo C, Moliterni AGG, Rizzi R. 2005. Space group determination: Improvements in EXPO2004. J Appl Crystallogr 38:760–767.
34. Altomare A, Camalli M, Cuocci C, Giacovazzo C, Moliterni AGG, Rizzi R. 2007. Advances in space-group determination from powder diffraction data. J Appl Crystallogr 40:743–748.
35. Thompson P, Cox DE, Hastings JB. 1987. Rietveld refinement of Debye–Scherrer synchrotron X-ray data from Al_2O_3. J Appl Crystallogr 20:79–83.
36. Finger LW, Cox DE, Jephcoat AP. 1994. A correction for powder diffraction peak asymmetry due to axial divergence. J Appl Crystallogr 27:892–900.
37. Allen FH, Watson DG, Brammer L, Orpen AG, Taylor R. 2006. Typical interatomic distances: Organic compounds. International Tables for Crystallography . Vol. C. Chapter 9.5, pp 790–811.
38. Stephens P. 1999. Phenomenological model of anisotropic peak broadening in powder diffraction. J Appl Crystallogr 32:281–289.
39. Fabian L, Kalman A, Argay G, Bernath GCs, Gyarmati Z. 2004. Two polymorphs of a beta-lactam (trans-13-azabicyclo[10.2.0]tetradecan-14-one). Concomitant crystal polymorphism and isostructurality. Chem Commun (Camb) 18:2114–2115.
40. Bendeif E, Dahaoui S, Francois M, Benali-Cherif N, Lecompte C. 2005. Isostructural phase transition in m-carboxyphenylammonium monohydrogenphosphite. Acta Crystallogr B 61:700–709.
41. Vujovic D, Nassinbeni L. 2006. Methyl paraben—A new polymorph? Cryst Growth Des 6:1595–1597.
42. Threlfall TL, Gelbrich T. 2007. The crystal structure of Methyl Paraben at 118 K does not represent a new polymorph. Cryst Growth Des 7:2297.
43. Klyne W, Prelog V. 1960. Description of steric relationships across single bonds. Experientia 16:521–523.
44. Kurahashi M, Fukuyo M, Shimada A. 1969. The crystal and molecular structure of carbazole. Bull Chem Soc Japan 42:2174–2179.
45. Chan HK, Doelker E. 1985. Polymorphic transformation of some drugs under compression. Drug Dev Ind Pharm 11:315–332.